sustainability

IMPACT FACTOR 3.3

CITESCORE 6.8

Article

Offshore Wind Farm Layout Optimisation Considering Wake Effect and Power Losses

José Baptista, Beatriz Jesus, Adelaide Cerveira and Eduardo J. Solteiro Pires

MDPI

https://doi.org/10.3390/su15139893

sustainability

MDPI

Article

Offshore Wind Farm Layout Optimisation Considering Wake Effect and Power Losses

José Baptista [1,2,*], Beatriz Jesus [1], Adelaide Cerveira [2,3] and Eduardo J. Solteiro Pires [1,2]

[1] Department of Engineering, University of Trás-os-Montes and Alto Douro, 5000-801 Vila Real, Portugal; al69759@alunos.utad.pt (B.J.); epires@utad.pt (E.J.S.P.)
[2] INESC-TEC UTAD Pole, 5000-801 Vila Real, Portugal; cerveira@utad.pt
[3] Department of Mathematics, University of Trás-os-Montes and Alto Douro, 5000-801 Vila Real, Portugal
* Correspondence: baptista@utad.pt

Abstract: The last two decades have witnessed a new paradigm in terms of electrical energy production. The production of electricity from renewable sources has come to play a leading role, thus allowing us not only to face the global increase in energy consumption, but also to achieve the objectives of decarbonising the economies of several countries. In this scenario, where onshore wind energy is practically exhausted, several countries are betting on constructing offshore wind farms. Since all the costs involved are higher when compared to onshore, optimising the efficiency of this type of infrastructure as much as possible is essential. The main aim of this paper was to develop an optimisation model to find the best wind turbine locations for offshore wind farms and to obtain the wind farm layout to maximise the profit, avoiding cable crossings, taking into account the wake effect and power losses. The ideal positioning of wind turbines is important for maximising the production of electrical energy. Furthermore,a techno-economic analysis was performed to calculate the main economic indicators, namely the net present value, the internal rate of return, and the payback period, to support the decision-making. The results showed that the developed model found the best solution that maximised the profits of the wind farm during its lifetime. It also showed that the location of the offshore substation played a key role in achieving these goals.

Keywords: nonlinear linear programming; offshore wind farm; optimisation; power losses; techno-economic analysis; wake effect

Citation: Baptista, J.; Jesus, B.; Cerveira, A.; Pires, E.J.S. Offshore Wind Farm Layout Optimisation Considering Wake Effect and Power Losses. *Sustainability* **2023**, *15*, 9893. https://doi.org/10.3390/su15139893

Academic Editor: Firoz Alam

Received: 2 May 2023
Revised: 8 June 2023
Accepted: 19 June 2023
Published: 21 June 2023

1. Introduction

Wind energy has been considered a key renewable source in Europe [1]. Its use is essential for achieving ambitious renewable energy goals and transforming the energy supply to one based on renewable energy [2].

According to the International Energy Agency (IEA), the world is facing a climate crisis, and all efforts are crucial. An increasing number of countries are committing to achieving zero carbon emissions by 2050, accounting for approximately 70% of global carbon emissions [3]. The wind sector has a target to increase its capacity by 390 GW by 2030.

The energy sector is the largest contributor to greenhouse gas emissions, and to combat this phenomenon and limit the global temperature increase to 1.5 °C until 2050, a fundamental transformation of energy production, transportation, and consumption is required. The Paris agreement commits countries to deep decarbonisation [4].

A recent study conducted by the European Union [5] highlights the untapped potential for offshore wind energy in Europe's seas. The aim is to increase energy wind 20-times, reaching 450 GW, with the goal of decarbonising energy and achieving carbon neutrality by 2050 [5]. At that point, it is projected that 15% of the capacity will be located in the South Seas and the remaining 85% in the North Seas, as estimated by [6].

One way to increase wind production, whether through onshore or offshore wind farms (WFs), is to optimise their layout. The optimisation of the WF layout is essential as it accounts for between 15% and 30% of the initial investment cost [7]. Several researchers have devoted their efforts to studying this topic; some works are referred to in the sequel.

Cerveira et al. [8] proposed an optimisation model to determine the optimal cable network layout considering only the cable infrastructure costs. Later, Cerveira et al. [9] presented different mathematical formulations for the optimal cable network architecture problem in onshore WFs. The aim was to reduce the total cost of infrastructure and energy losses while considering different cable types with different cross-sections. Even considering the energy losses, the effective choice of the decision variables enables obtaining a linear model. The inclusion of valid inequalities leads to more-efficient ILP models. Furthermore, the problem of simply minimising the infrastructure cost was addressed to evaluate the benefits of including the cost of energy losses. The same authors proposed other approaches for optimising the layout of onshore wind farms considering the energy losses and multiple substations [10] and, in another work [11], energy losses and duct sharing, which leads to significant savings.

Fischetti and Pisinger [12] proposed a mixed-integer linear programming (MILP) model to optimise the cable routing of offshore WFs respecting cable capacities, no-cross constraints, connection limits at the substation, and obstacles at the site. The objective was to minimise both the capital spent on cable and installation and the future reduced revenues due to power losses. They used both exact and metaheuristicmethods.

Balakrishnan et al. [13] stated that wind energy production depends on local conditions and the interference caused by nearby WTs. They used active wake control methods such as wake redirection control (WRC) and axial induction control (AIC) to reduce the wake effect and maximise power production in offshore wind farms. The wake effect negatively affects turbines that are placed too close together. A critical factor in the design of offshore wind farms (OWFs) is the distance between wind turbines (WTs) [14].

Therefore, the optimised placement of WTs should be made by considering the wake effect, as well as the cost of components within the wind farm (WF). The Jensen model is a simplified way of calculating wind speed, taking into account the wake effect, initially proposed by Jensen in [15]. The model was later improved in 1986 by Katic et al. [16] and is widely adopted in wind farm design. This model stands out for its performance and is one of the most-recommended [17].

Several authors have studied the WF position and the wake effect on energy production. Most techniques proposed are based on metaheuristics. Mirsane and Torabi [18] presented a method that calculates the WF input speed through wake interactions in a wind farm using a particle optimisation algorithm (PSO) to maximise energy production and to find the optimal wind farm layout. Amaral and Castro [19] considered the maximum energy production to minimise the levelised cost of energy. To achieve this, they used a genetic algorithm (GA) and a particle swarm optimisation technique to strategically place WTs bearing in mind the extraction of as much energy as possible. They considered only wake and internal network electrical losses. Horn [20] used a GA to find an optimal solution for the WF layout minimising wake effect losses.

In [21], a unified control of the active power optimisation of wind farms under the wake effect was proposed, which unifies the optimisation of kinetic energy in a low-wind-speed zone, the optimisation of the tilt angle and kinetic energy commitment in a moderate-wind-speed zone, and the optimisation of the tilt angle in a high-wind-speed zone between WTs.

Fischetti and Pisinger [22] argued that minimising establishment costs and increasing production profits in the design phase is crucial. Therefore, optimisation helps to increase production and reduce costs. They highlighted three crucial optimisation undertakings: turbine siting, electrical cable routing, and foundation optimisation. In Lima et al. [23], Jensen's model was used to calculate the wake effect only considering the predominant wind speed. From another perspective, the Jensen model was used to calculate the wake

effect considering all wind speeds obtaining the maximum energy production and the minimum levelised cost of energy (LCOE) [24]. This model enables the optimal positioning of WTs to achieve maximum energy efficiency while considering losses due to the wake effect. In [25], a deep neural network was used for optimal WT placement considering the wake effect. Taylor et al. [7] proposed combined algorithms based on ant colony optimization and a decomposition technique for large networks to optimise the layout design for offshore WFs. They compared the algorithm with other heuristics and exact algorithms and claimed that their algorithm was a good alternative for very large WFs.

Table 1 compares the optimisation algorithms found in the literature highlighting the features addressed in each model, in particular the technique used, the advantages/disadvantages, the wake effect, the location of the substations, and the power losses.

Table 1. Comparison of the papers that were reviewed.

Year	Refs.	Optimisation Algorithm	Advantages/Disadvantages	Wake Effect	Sub-Stations	Power Losses
2023	[7]	MILP	Gives the exact solution of the problem.		✓	✓
		AOC	Does not guarantee finding the optimal solution. The best solution found was 0.4–7.6% higher than the optimal solution.		✓	✓
		AOCsp	Does not guarantee finding the optimal solution. The best solution found was 0.0–1.4% higher than the optimal solution.		✓	✓
2023	[11]	ILP	Obtains the optimal solution of the problem.		✓	✓
2022	[13]	PSO	Does not guarantee finding the optimal solution.	✓		
2022	[23,24]	MILP	Gives the optimal solution to the problem.	✓		
2022	[25]	ML/DNN	Does not guarantee finding the optimal solution within an absolute error of 1.5%.	✓		
2021	[10]	ILP	Obtains the optimal solution of the problem.		✓	✓
2019	[22]	MILP	Obtains the optimal solution of the problem.	✓		✓
2018	[12]	MILP	Obtains the optimal solution of the problem.	✓	✓	✓
2018	[20]	GA	Does not guarantee finding the optimal solution.	✓		
2017	[19]	GA/PSO	Does not guarantee finding the optimal solution.	✓	✓	✓
2016	[9]	ILP	Obtains the optimal solution to the problem.		✓	✓

This paper presents the concepts necessary to evaluate electrical energy production from wind, considering the wake effect. A nonlinear optimisation model is presented, which allows not only the selection of the WT that will be part of the OWF final design, taking into account the wake effect, but also the connections between them and the type of cable used, considering the cost of the cables and energy losses. Furthermore, constraints avoiding cable crossings are included.

The novelty of this work is the exact approach to the simultaneous selection of the WT set and the design of the connections without cable crossings.

There are variables related to the existence or not of a WT at a site and variables related to the existence or not of a connection between WTs, obtaining a problem with binary variables. The goal was to maximise the profit obtained during the WF's lifetime. In the produced annual energy calculation, the wake effect between the existing turbines in the solution will lead to a nonlinear objective function, so a nonlinear model was obtained.

The manuscript is structured into six sections, including the Introduction. In Section 2, the importance of wind energy is analysed, and the methods of obtaining energy from wind are discussed. Section 3 addresses the main typologies for AC collection grids in offshore wind farms, discusses the transmission of the HVAC, and presents two AC concepts for wind farms and the energy losses in the network branches The nonlinear programming (NLP) model used for optimising the WF layout is presented in Section 4. The case studies

are addressed in Section 5, and the results obtained are presented and discussed. Finally, Section 6 highlights some conclusions.

2. Wind Resource

In order to evaluate electrical energy production, it is important to analyse the wind resource potential considering the technical and physical aspects that affect the WF energy production. This section addresses various aspects, in particular the Weibull wind speed distribution, the Prandtl logarithmic law, the wind power density, the thrust coefficient, and the Jensen model for the wake effect.

2.1. Weibull Wind Speed Distribution

To calculate the wind potential energy, it is essential to have knowledge of the wind distribution throughout the year. Although several probabilistic distributions portray the wind regime, the Weibull distribution is commonly considered the most-suitable [26–28]. The Weibull distribution model is given by Equation (1) in the wind direction σ, at WT j:

$$f_{W\sigma j}(u) = \frac{k}{c_{\sigma j}} \left(\frac{u}{c_{\sigma j}} \right)^{k-1} e^{-\left(\frac{u}{c_{\sigma j}}\right)^{k}}, \quad (1)$$

where k is a non-dimensional shape parameter, u is the wind speed, in m/s, and $c_{\sigma j}$ is the scale parameter, in m/s, in the wind direction σ at WT j given by:

$$c_{\sigma j} = \frac{2 \cdot \overline{u}_a}{\sqrt{\pi}}, \quad (2)$$

where $\overline{u}_a$ is the local annual mean wind speed.

The Weibull distribution reduces to the Rayleigh distribution, given by Equation (3), for $k = 2$. These models allow obtaining the annual wind speed distribution based solely on the knowledge of the local mean wind speed [27,29].

$$f_{R\sigma j}(u) = \frac{2}{c_{\sigma j}} \cdot \frac{u}{c_{\sigma j}} \cdot e^{-\left(\frac{u}{c_{\sigma j}}\right)^{2}}. \quad (3)$$

2.2. Wind Speed Extrapolation at Different Heights with Prandtl's Logarithmic Law

The friction between the wind and the Earth's surface results in a decrease in the wind speed. Thus, the wind speed increases proportionally with height due to the friction with the Earth's surface. Therefore, adjusting the recorded wind speed according to the vertical height of interest is necessary.

The importance of establishing a relationship between the instantaneous speed variation of the wind with height and the probability distribution parameters of the wind are discussed in [30]. The Prandtl logarithmic law [30] states:

$$u_0(z) = \overline{u}_r \frac{\ln \frac{z}{z_0}}{\ln \frac{z_r}{z_0}}, \quad (4)$$

where $u_0(z)$ is the mean wind speed at height z, $\overline{u}_r$ is the average speed recorded at reference height z_r, and z_0 is the soil roughness.

2.3. Energy Generated by Wind

Considering the wind profile and the WT power curve (Figure 1), it is possible to calculate the annual energy produced at WT j, in kWh, by the conversion system for a single wind direction using Equation (5).

$$AEP_j = 8760 \int_{u_0}^{u_\infty} P_{e_u} f_{R\sigma j}(u) du. \quad (5)$$

In this equation, $f_{R\sigma j}(u)$ is the Rayleigh probability density function, 8760 is the number of annual hours, and P_{e_u} is the WT power, in kW, for a u wind speed [31].

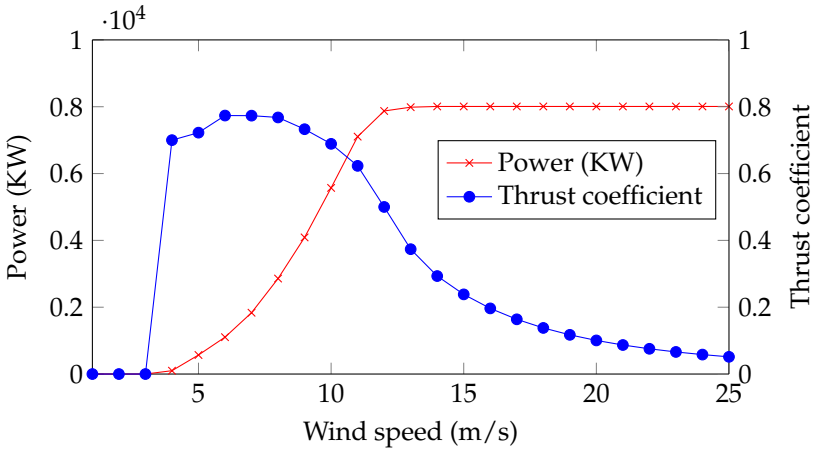

Figure 1. Power curve and thrust coefficient examples.

The wind resource at a particular location can be characterised by analysing the wind speed and direction data, known as wind knowledge. This information is critical in determining the dominant wind directions, which is essential in designing the WF configuration to minimise the wake effects and maximise energy production [32]. Using wind rose data, each wind direction can be associated with the Rayleigh distribution, estimating the wind distribution throughout the year. The inclusion of wind directions in the AEP leads to Equation (6), where σ_k represents the wind direction in degrees [31] and k ranges in $[0, 360]$ in k degrees.

$$AEP_j = 8760 \int_{\sigma_0}^{\sigma_{360}} \int_{u_0}^{u_\infty} P_{e_u} f_{R\sigma j}(u) du d\sigma. \quad (6)$$

To compute AEP_j, its approximate discrete distribution is considered, obtaining:

$$AEP_j = 8760 \sum_{\sigma=\sigma_0}^{\sigma_{360}} \sum_{u=u_0}^{u_\infty} P_{e_u} f_{R\sigma j}(u). \quad (7)$$

To determine the energy production of a wind farm, it is necessary to evaluate the reduction in the wind speed caused by upstream WTs on downstream turbines. The reduction in the wind speed due to the wake effect from upstream WTs is related to the thrust coefficient, C_t, of the upstream turbine. The thrust coefficient, also referred to as the drag coefficient, demonstrates a significant decrease as the wind speed increases, as depicted in Figure 1. The power output of a single WT is determined by its power curve, but for an array of WTs, the wake effects and power output are mainly determined by the thrust coefficient curve [31]. Figure 1 gives the power curve and the thrust coefficient of the WT used in this study.

2.4. Jensen Model for the Wake Effect

The conversion of kinetic energy from a moving air mass into mechanical energy by WTs depends on the wind speed. The wake effect, or the interference from the wind passing through one turbine to another, can impact the energy production of downstream turbines by reducing the air mass flow and wind speed. The Jensen model, as depicted in Figure 2, is a widely used approach for modelling the wake effect in wind farms [33,34].

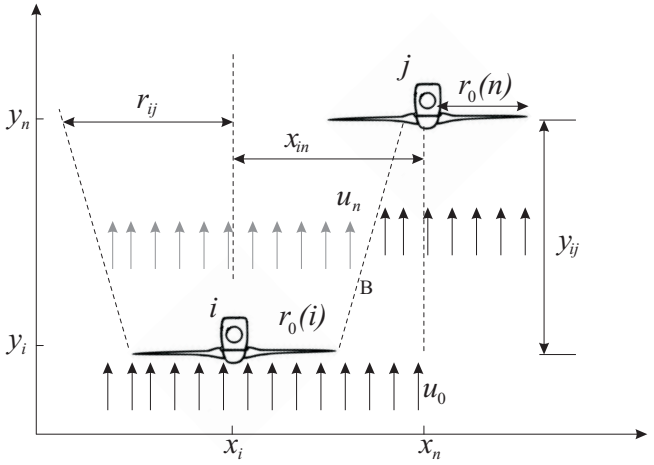

Figure 2. Principle of the *Jensen* wake effect model (top view).

The wake effect between two turbines is illustrated in Figure 2. The upstream turbine i and the downstream turbine j are located at coordinates (x_i, y_i) and (x_n, y_n), respectively. The wake effect is axisymmetric, and its intensity is dependent on the distance between the two turbines and the wind direction, as illustrated by the dashed line B and the wake radius r_{ij}. The wind speed at the downstream turbine j, u_j, is determined by:

$$u_j = u_0(z)\left(1 - \sqrt{\sum_{i \in N_j}\left(\frac{2a}{T_{ij}}\right)^2}\right), \tag{8}$$

$$T_{ij} = \left(1 + \alpha.\frac{y_{ij}}{r_{ij}}\right)^2, \tag{9}$$

$$r_{ij} = \alpha y_{ij} + r_0, \tag{10}$$

where N_j are the turbines that affect turbine j considering the wake effect phenomenon, r_0 is the radius of the upstream turbine, y_{ij} is the distance between turbines i and j, measured in the wind direction, and α is a dimensionless parameter and determines how fast the wake expands, given by [35]:

$$\alpha = \frac{1}{2\ln\left(\frac{z}{z_0}\right)}, \tag{11}$$

where z is the axis height and z_0 is the surface roughness length, whose value depends on the terrain characteristic. The value of roughness in water is usually 0.0002, although it may increase with sea conditions [34].

The reduction in the wind speed from the free-flow speed, $u_0(z)$, to the speed at the WT is represented by the axial induction factor, a, according to [35]:

$$a = \frac{1 - \sqrt{1 - C_t(u)}}{2}, \tag{12}$$

where $C_t(u)$ is the thrust coefficient, which varies with the wind speed [36].

When the overall wake effect is to be determined, all wind directions must be considered. For each wind direction, σ, the mean wind speed at WT j caused by the presence of multiple turbines is given by (8), adjusting the set N_j and the value of T_{ij} for the considered direction.

3. Electrical System Connections

3.1. Radial Topology

In offshore wind farm construction, alternating current (AC) collection grids are the widely accepted commercial standard. This section provides an overview of AC collection grids, specifically in the context of offshore wind power.

One of the most-used connection systems is the radial topology system, which will also be used in the case studies of this paper. In this topology, all WTs are connected to a single series circuit. The radial topology illustrated in Figure 3 shows the arrangement of offshore WTs connected in series to a feeder and collected in the manifold hub. The cable and generator ratings in a radial design have a restriction on the number of WTs that can be connected to a feeder. Because it has fewer cables overall than alternative designs, is less expensive, simple to use, and flexible enough to allow the cable capacity to be changed as the distance from the hub rises. This is due to the fact that each feeder transmits less power than the next [37].

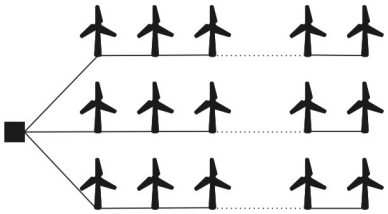

Figure 3. Radial topology.

3.2. Electrical System

Synchronised AC networks oscillating at the same frequency and in phase are connected by high-voltage alternating current (HVAC) transmission. Three-phase systems are preferred over one- or two-phase systems as they require less material for the same power transfer and provide the rotating magnetic field needed for the stator of electrical AC machines. Synchronous machines and induction machines have simpler configurations than DC machines, making them less expensive and easier to maintain. The power losses in an AC connection are proportional to the square of the current, while the power transferred is proportional to the square of the voltage. Hence, high voltage is desired for power transfer [37].

The electrical system of an offshore wind farm can be divided into three parts: the collection system, the integration system, and the transmission system. The collection system transports the energy generated by turbines to a central collection point. In some cases, several WT clusters may be connected by integration cables to a minor substation. If the electrical losses warrant it, the collection system or the integration system (if it exists) can be connected to a main offshore substation, which transmits the energy to shore [19].

The collecting cable, also referred to as the array cable, begins with a transformer installed at each WT, which steps up the generation voltage from typically 690 V to a medium voltage, typically ranging from 25 kV to 40 kV [38].

Integrated cable solutions for offshore wind farms are HVAC submarine cables ranging from 123 kV to 420 kV with various available designs: qualified for up to 420 kV for single and three-core XLPE cables [39].

Currently, all WFs are built using AC technology for the grid and transmission system. Two AC concepts are presented in the following: the small AC WF and the large AC WF [37].

3.2.1. Small AC Wind Farm

For small WFs located near the shore, the connection grid connects the WTs and transfers power from the WF to the grid interface. This approach is the most usual. The connection grid is used to connect the WTs and link them to the shore, as illustrated in Figure 4. The voltage level of these WFs relies on the distance to the shore and the power capacity of the wind farm, as reported in [37].

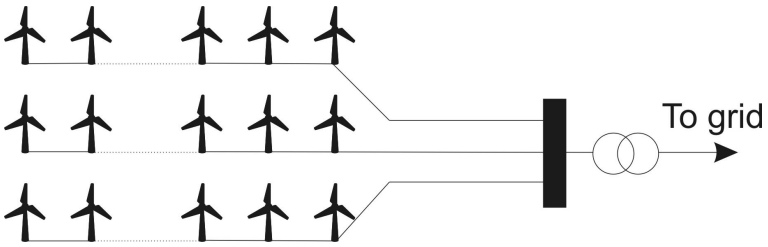

Figure 4. Small AC wind farm layout.

3.2.2. Large AC Wind Farm

The large AC WF is linked to an offshore substation, where reactive power compensation devices are built, and the voltage is tuned to minimise transmission losses. As shown in Figure 5, the voltage levels depend on the power rating and distance from the coast of the WF. This strategy is suitable for quite sizeable WFs that are far from the shore. However, the distance from the coast limits the AC transmission system's ability to carry data, which places physical constraints on it. Using a low-frequency AC network and lowering the offshore frequency are two potential solutions to this problem [37].

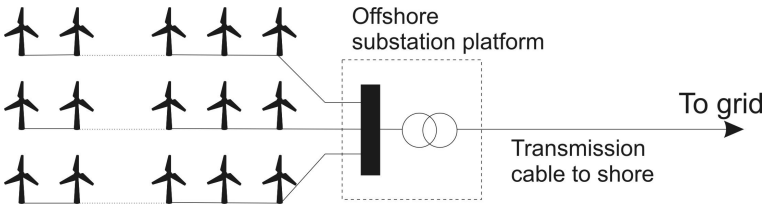

Figure 5. Large AC wind farm layout.

3.3. Line Losses Modelling

In offshore WFs, to ensure a viable grid arrangement, it is crucial to keep the voltage drop within regulatory limits and minimise power losses. As in the collecting network, the distances between WTs and between WTs and the substation is usually short (of the order of hundreds of meters), then the voltage drop remains within the regulatory limits. Furthermore, the short line model can be used, where the transmission line model considers only the series impedance and neglects the shunt admittance, as shown in Figure 6.

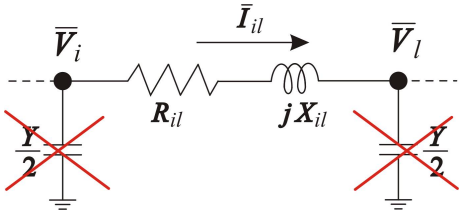

Figure 6. Electrical branch line equivalent neglecting the shunt admittance.

An economic assessment of an offshore wind farm must consider the power losses during its lifetime. The power losses in each connection depend on the characteristic cable used. Each cable is characterised by the voltage level, the power limits, the resistance, and the costs. Table 2 presents the available cable set considered in this study.

Although the power losses include a reactive and active component, the reactive component can be neglected in the case of short lines, as was done in this work. The active power losses in a (i, l) cable connection, P_{il}, can be given by:

$$P_{il} = \ell_{il}.\left(R_k.I_{il}.l_f\right)^2 \tag{13}$$

where ℓ_{il} is the length of the connection; R_k is the resistance per unit length of the cable type k used in this connection; I_{il} is the current crossing connection (i, l), which is the sum

of the currents generated by all WTs that are supported by (i, l); and l_f is the load factor, which is the average power generated by the WT divided by its peak capacity [9].

Table 2. Cable characteristics.

Voltage, U (kV)	Type k	Section (mm^2)	Current Rating, I_{z_k} (A)	Electrical Resistance, R (Ω/km)	Cost (M EUR/Km)
33	1	120	318.4	0.14	0.31
	2	150	355.1	0.11	0.32
	3	185	398.8	0.09	0.34
	4	240	458.3	0.07	0.37
	5	300	531.8	0.06	0.40
	6	400	593.0	0.04	0.44
	7	500	664.8	0.03	0.49
	8	630	706.8	0.03	0.52
	9	800	775.0	0.02	0.59

The WTs were considered to have a unity power factor in this paper, i.e., $\tan \varphi = 0$, which means that the current and voltage they draw into the network are in phase, or $\varphi = 0$. The rated current, I_r, drawn by each WT is given by:

$$I_r = \frac{P_r}{\sqrt{3} \cdot U} \tag{14}$$

where U is the voltage of the interconnection grid and P_r is the rated power of the WTs.

4. Optimisation Model

This section presents the optimisation model to obtain the optimal layout of OWFs, determining the optimal set of WTs to be considered in the final design, as well as the connections and the cable type used. It is a nonlinear programming (NLP) model with integer variables.

4.1. Datasets and Parameters

Consider the node sets $N = \{1, \ldots, n\}$ as the possible locations of WTs and a substation location, Node 0.

The goal was to determine the set of locations $N' \subseteq N$ to install WTs and, simultaneously, find the WF connection layout, i.e., a spanning tree of a graph $G = (V, A)$ with $V = N' \cup \{0\}$, and $A = \{(i, j) : i \in V, j \in N'\}$, the substation node being the root of the spanning tree. The substation will be connected directly to turbines by several cables. Each of these cables will connect some WTs, which in turn will be connected to other WTs. A set of WTs connected to each other by a cable coming from the substation and its connections is called a branch line. Usually, these turbines are connected in series.

This work considered a set $K = \{1, \ldots, n_k\}$ of the available cables, whose characteristics are listed in Table 2. The number of WTs in each branch line is bounded according to the maximum value for the current intensity of the cables. For a cable type k, the maximum current intensity value I_{z_k} imposes an upper bound for the number of downstream WT given by $\left\lfloor \frac{I_{z_k}}{I_r} \right\rfloor$. Therefore, the maximum number of WTs in any branch line is given by:

$$Q = \max_{k \in K} \left\lfloor \frac{I_{z_k}}{I_r} \right\rfloor, \tag{15}$$

where I_r is the rated current drawn by each WT, given by Equation (14). Furthermore, $Q(i)$ being the maximum number of WTs that a location i can support, it holds that $Q(0) = Q$ and $Q(i) = Q - 1$, for $i \in N$.

For a WT installed at location i, let $AEP(i)$ be the annual energy produced by itself, considering the wake effect, obtained according to Equation (7).

The energy cost, c_e, in EUR/MWh, is a known parameter, according to the Portuguese market.

4.2. Revenues and Costs

The net profit is the difference between the revenues and the total costs. As revenues, we have the income from the sale of energy. The amount sold is the energy generated minus the active losses in the energy transmission process during the expected wind farm lifetime. Therefore, we can consider as costs the sum of the WT costs, c_w, the cable cost, c_c, and active losses costs, c_p, and as income received from the sale of all the energy generated by the WTs, AEP, during the wind farm lifetime.

Let AEP_i be the annual energy generated by WT i, in MWh, obtained through Equation (7). Without considering the power losses, the income received from the sale of all the energy produced during the WF's lifetime, 20 years, is given by:

$$20 \cdot \sum_{i \in N} x(i) \cdot AEP_i \cdot ce \tag{16}$$

The obtained optimisation model is nonlinear due to the expression of AEP_i, which is nonlinear on variables x with respect to the wind speed considering the wake effect, Equation (8) for the WTs in the solution.

The amount of power generated is independent of the type of cable used in the connections. Therefore, in order to maximise the profitability of the wind farm, the type of cable used in each connection can be calculated in advance and should minimise the cost of links, CL, which includes the cable costs and the active losses' costs. This value depends on the maximum cable capacity, which in turn depends on the number of downstream turbines.

Using Equation (13), the cost of the active losses, during the wind farm lifetime, in a connection $(i, j) \in A$ supporting t downstream turbines, using a three-phase cable of type k is

$$c_{p_{ij}}^{kt} = 3 \cdot h \cdot c_e \frac{\ell_{ji} \cdot R_k}{1000} \cdot t^2 \cdot l_f^2 \cdot I_r^2, \tag{17}$$

where h is the number of hours during the expected wind farm lifetime (20 years), c_e is the energy cost, ℓ_{ij} is the distance, in meters, between turbines i and j, R_k is the resistance of the cable type k, I_r is the rated current drawn by a WT, and l_f is the load factor, which reflects the real operating conditions during the wind farm lifetime.

The cable cost to make the connection (i, j) using a cable of a type k is

$$c_{c_{ij}}^{k} = 3 \cdot c_k \cdot \ell_{ij},$$

where $3 \cdot c_k$ is the three-phase cable cost (EUR/m).

Following [9], a preprocessing calculus was performed to determine the optimal cable type, k_{ij}^t, for a connection (i, j) supporting the current of t downstream wind turbines:

$$k_{ij}^t = \arg \min_{k \in K : t \cdot I_r \leq I_{z_k}} \left(c_{c_{ij}}^{k} + c_{p_{ij}}^{kt} \right), \tag{18}$$

and the corresponding cost:

$$CT_{ij}^t = c_{c_{ij}}^{k_{ij}^t} + c_{p_{ij}}^{k_{ij}^t} \tag{19}$$

is the minimum cost for the connection (i, j) with t downstream turbines.

4.3. Decision Variables

The decision variables are:

- For all $i \in N$, binary variables x_i taking a value of 1 if the WT at location i is in the solution; otherwise, it takes a value of 0.
- For all $i \in N'$ and $j \in N$, binary variables y_{ij}^t taking a value of 1 if the nodes i and j are connected (node i being on the substation side) and support the current of t downstream WTs (including the one located at j); otherwise, it takes a value of 0.

4.4. Cable Connection Layout Model

The NLP model to optimise the wind farm layout considering the choice of the WT and the connection layout, WFL, is given by:

$$\max \quad 20 \cdot \sum_{i \in N} x_i \cdot AEP(i) \cdot ce - \sum_{i \in N} x_i \cdot cw - \sum_{i \in N'} \sum_{j \in N} \sum_{t=1}^{Q(i)} CT_{ij}^t \cdot y_{ij}^t \tag{20}$$

subject to

$$x_i + x_j \geq 2 \cdot \sum_{t=1}^{Q(i)} y_{ij}^t, \; i, j \in N, i \neq j \tag{21}$$

$$x_j \geq \sum_{t=1}^{Q} y_{0j}^t, j \in N \tag{22}$$

$$\sum_{i \in N} \sum_{t=1}^{Q} \left(t \cdot y_{0j}^t \right) = \sum_{i \in N} x_i \tag{23}$$

$$\sum_{i \in V} \sum_{t=1}^{Q(i)} y_{ij}^t = x_j, j \in N \tag{24}$$

$$\sum_{i \in V} \sum_{t=1}^{Q(i)} \left(t \cdot y_{ij}^t \right) = \sum_{i \in N} \sum_{t=1}^{Q(i)} \left(t \cdot y_{ji}^t \right) + x_j, j \in N \tag{25}$$

$$\sum_{i \in \mathcal{N} \cup \{0\}} \sum_{\tau=t+1}^{Q(i)} \left(\left\lfloor \frac{\tau - 1}{t} \right\rfloor \cdot y_{ij}^\tau \right) \geq \sum_{i \in N} \sum_{\tau=t}^{Q-1} y_{ji}^\tau, j \in N, t = 2, \ldots, Q-2 \tag{26}$$

$$y_{0j}^Q \geq \sum_{i \in N} y_{ji}^{Q-1}, j \in N \tag{27}$$

$$x_i \in \{0,1\}, i \in N \tag{28}$$

$$y_{ij}^t \in \{0,1\}, i \in N', j \in N, t = 1, \ldots, Q(i) \tag{29}$$

The objective function (20) maximises the incomes of the layout. Constraints (21) link variables x and variables y, ensuring that a connection between two locations i and j can only exist if there are WTs installed on both sites. Constraints (22) are a special case of the previous one for the links from the substation, ensuring that a link between the substation and a location j can only exist if there is a WT installed at this location. Constraint (23) guarantees that the network connects all the selected WTs. Constraints (24) guarantee that each WT has one incoming connection. Constraints (25) are the flow conservation constraints and guarantee that, for each WT $j \in N$, if an incoming connection supporting t downstream WTs exists, then the outgoing connections from WT j must support $t-1$ downstream WTs. Constraints (26) and (27) are valid inequalities, able to improve the model efficiency, proposed in [9]. These constraints reflect the fact that, if a connection supports τ downstream wind turbines, then the number of connections outgoing from node j supporting t or more downstream wind turbines cannot be higher than $\left\lfloor \frac{\tau-1}{t} \right\rfloor$.

Finally, Constraints (28) and (29) are the variable domain constraints.

4.5. Avoiding Crossing Cables

The model WFL, (20)–(29), does not contain constraints to avoid crossing cables. In the design of offshore wind farms, this is an aspect to take into account [40–42].

The number of possible crossings is too large. It would be unreasonable to include all the corresponding constraints. Therefore, an iterative process was used to solve the problem, where after obtaining a solution, a test was performed to evaluate the existence of crossings, and if this is the case, constraints to avoid the obtained crossings are included. The process is repeated until a solution with no crossings is obtained or until the limit of the number of iterations has been reached.

There is a crossing between two connections (i, j) and (k, l) if there is a (inner) point of intersection of the two corresponding line segments. Let (x_i, y_i), (x_j, y_j), (x_k, y_k), and (x_l, y_l) be the coordinates of the non-collinear locations i, j, k, and l, respectively. There is a crossing if α_1 and α_2 exist such that:

- $\alpha_1, \alpha_2 \in [0, 1]$
- $\alpha_1 \cdot (x_i, y_i) + (1 - \alpha_1) \cdot (x_j, y_j) = \alpha_2 \cdot (x_k, y_k) + (1 - \alpha_2) \cdot (x_l, y_l)$

5. Computational Results

In this section, the case study is presented in four situations. The first is with the substation 2 km from the OWF, the second with the substation in the centre of the OWF, and the last two with the substation at the top and bottom right.

The obtained results with the NLP model, presented in Section 4, to maximise the incomes of the layout are presented and discussed, as well as the effectiveness of the developed optimisation model. The computational tests were performed using an Intel(R) Core(TM) i7-855OU CPU @ 1.80 GHz 1.99 GHz with 8 GB of RAM and using the software Xpress 8.8 with Xpress-Optimizer 35.01.01 and Xpress-Mosel 5.0.2 [43].

5.1. The Case Study

The turbines used were Vestas v164-8.0, a widely used Danish turbine in offshore wind farms, with the specifications listed in Table 3 [44,45].

Table 3. Wind turbine specifications—Vestas v164-8.0.

Vestas v164-8.0 WT	Specifications
Rated power (MW)	8
Cut-in wind speed (m/s)	4
Cut-out wind speed (m/s)	25
Rotor diameter (m)	164
Blades' swept area (m^2)	21,124
Shaft height (m)	140
Cost (EUR M)	12

The turbine power curve provided by the manufacturer is shown in Figure 1. The curve analysis showed that the wind turbine started operating at a wind speed of 4 m/s and reached its maximum power of 8 MW at a wind speed of 13 m/s. This maximum value remained constant up to 25 m/s, which is a safe operating limit.

The location of the turbines was selected to be 20 km from the coast of Viana do Castelo, Portugal, where, according to the Portuguese government, a cluster with a maximum expected power of 2 GW could be installed. The map of Figure 7 shows the proposed location.

Figure 7. Location of the proposed OWF, marked red.

The arrangement of the turbines in the offshore wind farm proposed in this study was in a configuration of 8×8, 64 equally spaced WTs, with a maximum installed power of 512 MW, which is depicted in Figure 8. With respect to the substation location, four scenarios were considered: one with a peripheral substation (SC1) at position $(9000, 4000)$, the second with a central substation (SC2) at position $(3500, 3500)$, and the other two scenarios with the substations at positions $(5500, 6500)$ and $(5500, 500)$.

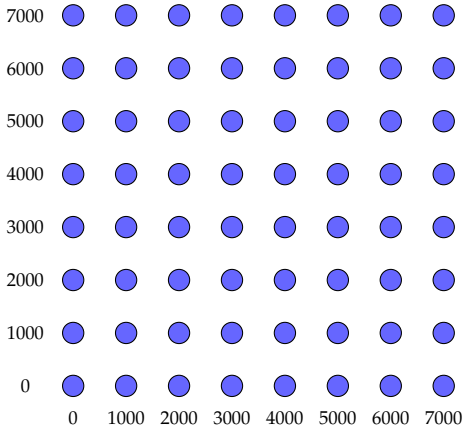

Figure 8. Possible location of the WT.

The wind resource used was obtained from the Global Wind Atlas [46]. The average annual wind speed of 8.43 m/s was obtained at a height of 100 m and used in the analysis. Figure 9 shows the wind speed rose and wind frequency rose obtained from the Global Wind Atlas. The wind speed rose indicates that the wind predominantly blows from the north (0°); see Figure 9a. The relative frequency of occurrence in the direction of 330° is 13%, as depicted in Figure 9b. The horizontal and vertical distances between adjacent sites were set to 1000 m.

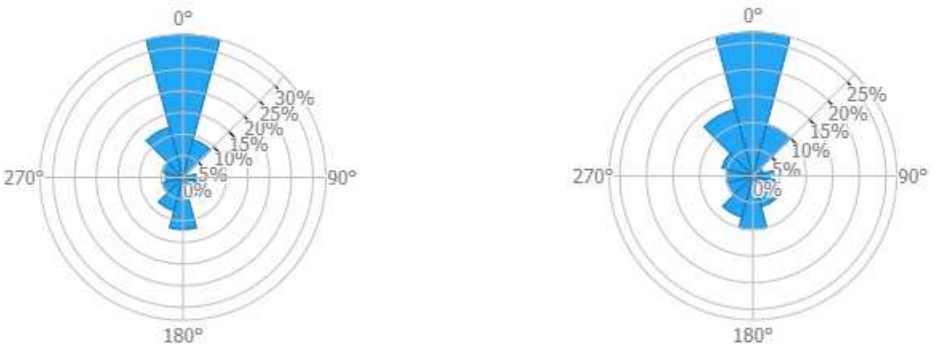

(**a**) (**b**)

Figure 9. Wind rose. (**a**) Average speed, 8.43 m/s. (**b**) Frequency.

The average wind speeds were measured at a height of 100 m. To adjust the wind data to the turbines' rotor height of 140 m, the Prandtl law was used, given by Equation (4).

The Jensen model for the wake effect was applied to calculate the upstream wind speed in each turbine (u_j), as depicted in Figure 2. The energy production of each turbine differed, as not all turbines received the same wind velocity. By using the thrust coefficients (Figure 1) and applying Equations (8) and (9), the wind speed (u_j) was calculated, and it was observed that the energy produced by each turbine decreased based on the wind direction, if all turbines were installed.

The radial topology was chosen for the development of the offshore wind farm (OWF); see Figure 3.

The cables used in the electrical collecting system for the OWF were XLPE Submarine Cables. The properties of the available cable types for this study are characterised in Table 2 [47], where the cable cost, in the last column, includes the installation cost.

As the rated power of each WT was 8 MW and the voltage of the interconnection grid was $U = 33$ KV (see Table 2), the rated current of each WT was $I_r = 139.96$ A. According to the maximum value for the cable current rating, $I_{z9} = 775$ A, the maximum number of WTs in any branch line was $Q = \left\lfloor \frac{775}{139.96} \right\rfloor = 5$.

Concerning the price of energy, it was considered $c_e = 83.88$ EUR/MWh, and the value of the load factor, to be used in Equation (17), was $l_f = 0.5$ [48].

5.2. Results and Discussion

The optimisation model proposed in Section 4 was solved using the Xpress Optimizer 5.01.01, and the total running times of the four scenarios were 15,290.2, 1407.4, 1104.8, and 8711.5 seconds.

Figure 10 illustrates the obtained optimal solution for the SC1 scenario. In the figure, the substation is pink, the WTs blue, and the places not used are blue and grey, respectively. The final solution used 56 WTs with a total of 64 possible locations. The eight positions with no WTs were in the middle along the horizontal axis. The connections are drawn in black lines.

There were two pairs of branch lines: {0–32–20–19–18–17, 0–31–29–34–33–25} and {0–46–52–59–58–47, 0–40–47–54–53} with connections in a row (parallel), 0–32 and 0–40, respectively. Therefore, to distinguish the branch lines, the WTs of one branch line of each pair are shaded in blue.

Figure 11 illustrates the optimal solution where the substation is at the WF's centre, SC2 scenario. This solution used 60 WTs, 4 more WTs than the solution considered in the SC1 scenario. In this case, the vacant places were in the middle of the WF, where the wake effect had more impact. Note that these four places with no WTs were also vacant in the SC1 scenario.

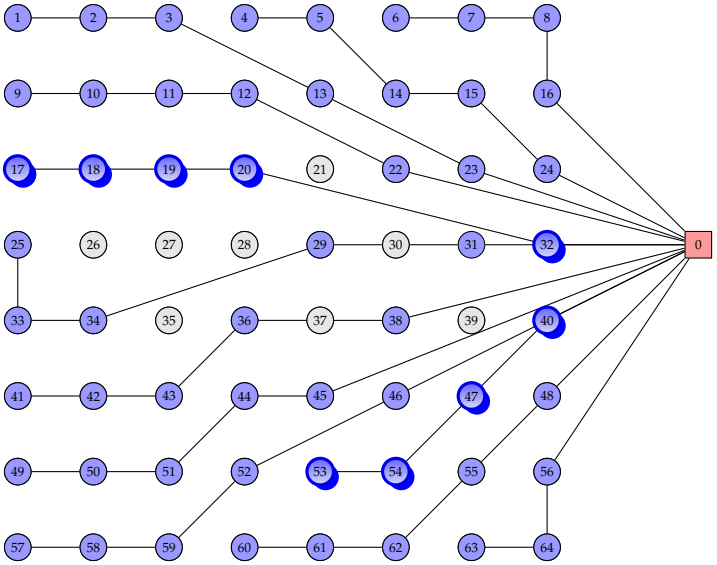

Figure 10. Optimal solution for peripheral substation, SC1 scenario (the WTs are blue, and the substation is pink).

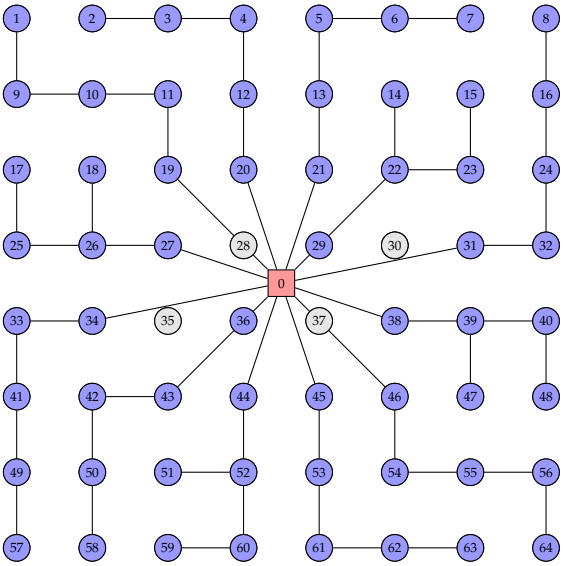

Figure 11. Optimal solution for central substation, SC2 scenario (the WTs are blue, and the substation is pink).

Figure 12 illustrates the optimal solution, where the substation is on top near the far right, the SC3 scenario. This solution used 58 WTs. It should be noted that these six places with no WTs were also vacant in the SC1 scenario.

Figure 13 illustrates the optimal solution where the substation is on the bottom near the far right, the SC4 scenario. This solution used 53 WTs. The vacant places were in the middle of the WF, where the wake effect had more impact. It should be noted that these six places with no WTs were also vacant in the SC1 scenario.

The characterisation of the optimal layout in terms of the number of WTs, used cables, and branch lines (BLs), considering all scenarios, is given in Table 4. The first column presents the scenario; column "# of WTs" has the number of WTs in the optimal solution. The following nine columns, from "1" to "9", present the number of connections with the correspondent cable type. Column "BLs" shows the number of branch lines. Finally, the last five columns indicate the number of branch lines with 1, 2, 3, 4, and 5 WTs (the cases drawn by the model).

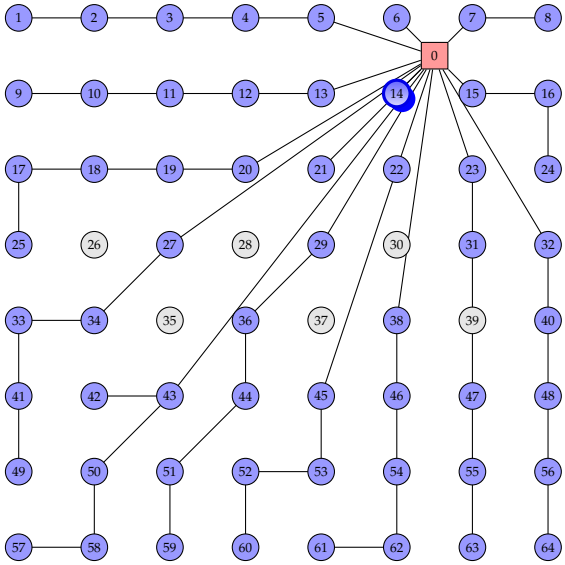

Figure 12. Optimal solution for top-far-right substation, SC3 scenario (the WTs are blue, and the substation is pink).

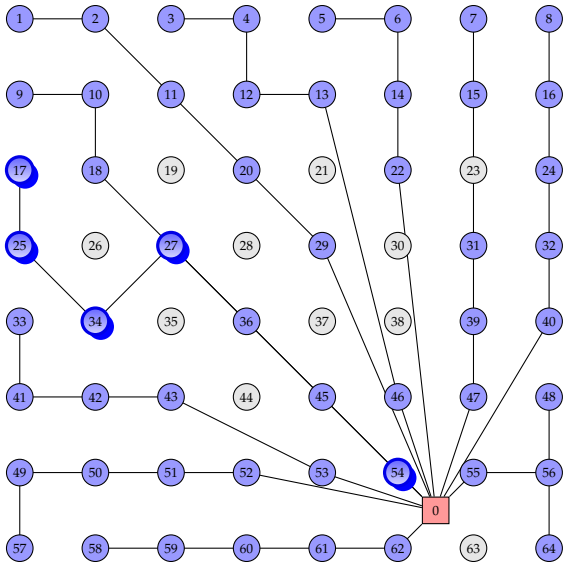

Figure 13. Optimal solution for botton-far-right substation, SC4 scenario (the WTs are blue, and the substation is pink).

Table 4. Optimal results—layout characterisation.

Scenario	# of WTs	Cable Type									BLs	No. of WTs/BL				
		1	2	3	4	5	6	7	8	9		1	2	3	4	5
SC1	56	24	0	0	12	0	11	0	9	0	12	0	0	1	2	9
SC2	60	28	0	0	0	0	12	0	12	0	12	0	0	0	0	12
SC3	58	28	0	0	11	0	9	0	10	0	15	3	1	1	0	12
SC4	53	22	0	0	11	0	11	0	9	0	11	0	0	0	2	9

Analysing Table 4, three cables were used when the substation was in the centre, Scenario SC2, and four cable types were used in the other scenarios. In all cases, the most-used cable was Type 1, which was used in connections with one or two downstream turbines. In Scenarios SC2 and SC3, the use of the Type 1 cable was more pronounced because the topology of the solution, SC2, was more branched (at the ends), and Solution SC3 had more branch lines and, therefore, more nodes supporting up to two descendants.

The number of branches varied from 11 in the SC4 scenario to 15 in the SC3 scenario. In the SC2 scenario, all the branches had five WTs, the highest possible value, while in the other scenarios, there were branches with fewer WTs, with 1, 2 3, and 4 WTs.

Table 5 presents the financial performance of the WF for all scenarios. Namely, the costs: turbines, c_w; cables, c_c; and power losses during the WF's lifetime (20 years), c_p; as well as the annual energy produced, AEP; the gross income over 20 years, revenue; and the net profit over 20 years, Opt. value.

Table 5. Optimal results: produced energy, costs, and revenues.

Sc.	Costs (EUR)			AEP	Revenue	Opt. Value
	c_w	c_c	c_p	(MWh)	(EUR)	(EUR)
SC1	672,000,000	125,564,878	12,996,490	1,256,168.4	209,435,1678	1,296,786,800
SC2	720,000,000	83,432,146	8,073,575	1,283,514.9	2,145,151,075	1,341,718,929
SC3	696,000,000	100,562,619	9,904,022	1,270,475.5	2,121,445,693	1,324,883,074
SC4	636,000,000	94,618,243	9,624,933	1,223,522.5	2,042,956,468	1,312,338,226

Figure 14 presents a bar chart with the three cost components, c_w, c_c, and c_p, for all scenarios. The total costs in the first three scenarios were very close, being EUR 810,561,368 for Scenario SC1, EUR 811,505,722 for Scenario SC2, and EUR 806,466,641 for Scenario SC3. In Scenario SC4, the total cost was lower, EUR 740,243,176, in accordance with the reduced number of WTs.

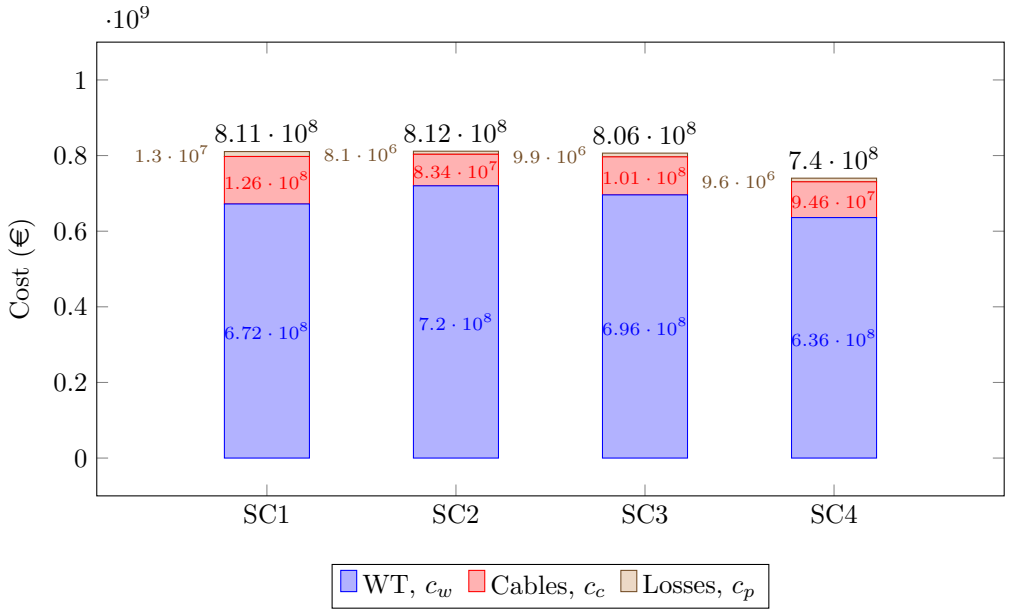

Figure 14. Bar chart costs of all scenarios.

Analysing Table 5, in all scenarios, the cost of the turbines represented the highest cost, varying between 78.5% and 88.8% of the total costs for Scenarios SC4 and SC2, respectively.

Comparing the two boundary scenarios, SC1 and SC2, although there was an increase of 7.1% in the WTs' costs with the SC2 scenario, there was only an increase of 0.12% in the total costs. Regarding cable costs and losses' costs, considering the substation in the centre, Scenario SC2, we obtained a cost reduction of 33.6% and 37.9%, respectively. This fact is in accordance with the layout obtained in the SC2 scenario, where the connections were shortened due to the substation's central position. Furthermore, during the WF's lifetime, the average annual production per WT in Scenario SC1 was 22.4 GWh and in Scenario SC2 was 21.4 GWh. As expected, the more turbines that were selected, the higher the reduction of the production by the wake effect.

5.3. Economic Analysis

The project's profitability was analysed using economic indicators for evaluating investments, namely the net present value (NPV), internal rate of return (IRR), and payback period (PBP). The NPV is the difference between cash inflows and cash outflows, called cash flows, updated over the project's life. If the $NPV > 0$, the investment would add value and can be accepted. On the other hand, if the $NPV < 0$, the investment would subtract value, and the project can be rejected. The IRR measures the expected return on investment and must be higher than interest rates. The PBP period refers to the time it takes to recoup the cost of an investment, so shorter payback periods mean more attractive investments. The values of the NPV, IRR, and PBP (payback) can be computed by Equations (30)–(32), respectively.

$$NPV = \sum_{j=1}^{n} \frac{R_j}{(1+i)^j}, \tag{30}$$

$$\sum_{j=1}^{n} \frac{R_j}{(1+IRR)^j} - I_t = 0, \tag{31}$$

$$\sum_{j=1}^{PBP} \frac{R_j}{(1+i)^j} \geq I_t, \tag{32}$$

where R_j is the net cash flow for the year j, with $j \in \{1, \ldots n\}$, n is the OWF's lifetime, I_t is the initial investment based on all the installations and equipment involved at the beginning of the OWF project, and i is the discount rate (in %), usually considered 7% for this type of investment [49].

Figure 15 illustrates the amortisation over the lifetime of the project. It is possible to analyse the return on investment over the OWF's lifetime, which is 20 years. In Scenarios CS1, CS2, and CS3 the return on investment was from the ninth year on, while in Scenario SC4, the return on investment began in the eighth year.

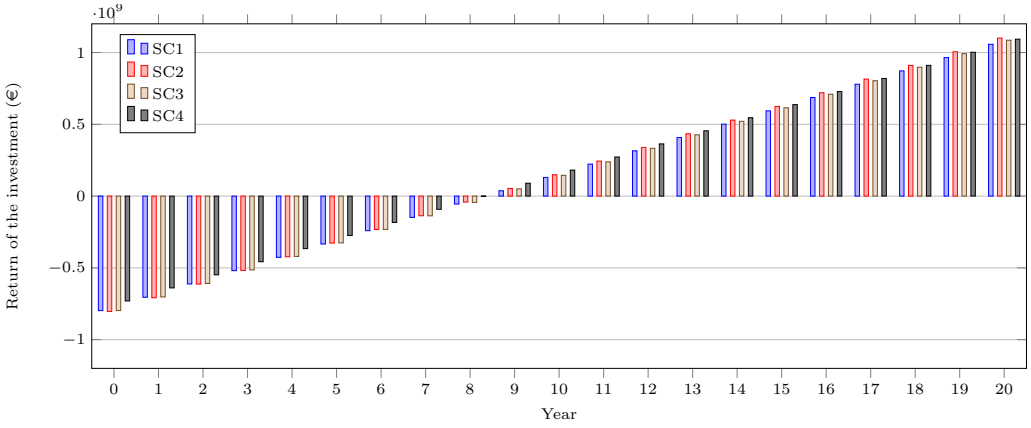

Figure 15. Amortisation results over the project's lifetime.

Table 6 presents the main economic indicators: NPV, IRR, and PBP. The SC1 scenario had the lowest NPV and IRR and the highest PBP. In contrast, the SC4 scenario had the highest NPV and IRR and the lowest PBP. These differences are likely to be related to the fact that the installation of turbines requires large investments and that the highest number of turbines were installed in Scenario SC2 (60) and the lowest number of turbines installed in Scenario SC4 (53).

It should be noted that, in Scenario SC4, as fewer turbines were installed, the reduction in production due to the wake effect was smaller, and the average annual production per WT was the highest. The average annual production per WT for Scenarios SC1, SC2, SC3, and SC4 was 22.4, 21.4, 21.2, and 23.1 GWh, respectively.

Table 6. Economic indicators.

Scenario	NPV (EUR)	IRR (%)	PBP (Years)
SC1	185,073,492.53	9.85	8.60
SC2	205,182,332.33	10.13	8.44
SC3	200,586,739.94	10.09	8.46
SC4	235,434,552.32	10.91	8.01

6. Conclusions

The focus on wind power continues to be a priority for decarbonising the planet. One of the ways to increase the wind power weight in the global energy mix is to take advantage of the sea as a resource that presents very advantageous conditions. Given that investments in offshore wind power are of greater magnitude than onshore, it is essential to assess which solutions are most-suitable for each location to maximise the return on investment. The study presented in this paper showed that optimising the site of wind turbines and offshore substations plays a key role in the efficiency of offshore wind farms. Furthermore, in addition to choosing the location of the turbines, the wind farm layout was also optimised by deciding which connections to make and which cable to use for those connections. A nonlinear optimisation model was proposed to solve the problem, avoiding connection crossings and considering the wake effect and power losses. The proposed model was applied to obtain the layout of a WF located along the northern coast of Portugal, Viana do Castelo.

Four scenarios were considered: one with the substation outside the OWF and the other three with the substation within the area of the WT deployment, in the centre, at the top right, and bottom right of the OWF. In all situations, there were locations with no WT installation due to the wake effect.

Regarding net profit, the central location of the substation, Scenario SC2, was more advantageous. The total cost was higher than in the other scenarios, and the total energy produced was higher due to the greater number of WTs installed, resulting in a 3.5% increase in profit compared to the SC1 scenario. However, using other indicators, the SC4 scenario was more advantageous. Therefore, it is important to perform an economic analysis by computing the main indicators to see how much the initial investment pays off. In fact, the economic analysis was paramount in this project based on renewable energy sources.

The analysis of the results obtained for the four scenarios studied allowed us to conclude that the most-efficient layouts were those that sited the substation within the area of the deployment of the turbines, preferably in the centre, and the substation further away from the predominant wind direction. Although Scenario SC2 had a higher profit value over the 20 years, the economic indicators showed that Scenario SC4 was the most-profitable option with an NPV of EUR 235,434,552.32, an IRR of around 11%, and a PBP of 8 years.

In this study, a very conservative lifetime was considered for the OWF (20 years), given that the vast majority of studies consider 25 years. We chose to consider a lower value as there is currently no history that allows us to say with certainty that offshore wind farms have such a long lifetime, given the external conditions to which all elements are subjected. If the lifetime of the OWF were to increase, the economic indicators would tend to improve more.

Author Contributions: Conceptualisation, J.B., B.J., A.C. and E.J.S.P.; methodology, J.B., B.J., A.C. and E.J.S.P.; software, B.J. and A.C.; validation, J.B., B.J., A.C. and E.J.S.P.; formal analysis, J.B., B.J., A.C. and E.J.S.P.; investigation, J.B., B.J., A.C., and E.J.S.P.; resources, J.B., B.J., A.C. and E.J.S.P.; writing—original draft preparation, J.B., B.J., A.C. and E.J.S.P.; writing—review and editing, J.B., B.J., A.C. and E.J.S.P.; visualisation, J.B., B.J., A.C. and E.J.S.P.; supervision, J.B., A.C. and E.J.S.P. All authors have read and agreed to the published version of the manuscript.

Funding: This research received no external funding.

Conflicts of Interest: The authors declare no conflict of interest.

Abbreviations

The following abbreviations are used in this manuscript:

AC	Alternating current
AIC	Axial induction control
AOC	Ant colony optimisation
AOCsp	Ant colony optimisation with decomposition
BL	Branch line
CS	Central substation
DC	Direct current
DNN	Deep neural network
GA	Genetic algorithm
HVAC	High-voltage alternating current
IPL	Integer linear programming
LCOE	Levelised cost of energy
IRR	Internal rate of return
MILP	Mixed-integer linear programming
ML	Machine learning
NLP	Nonlinear programming
NPV	Net present value
OWF	Offshore wind farm
PBP	Payback period
PS	Peripheral substation
PSO	Particle swarm optimisation
WF	Wind farm
WRC	Wake redirection control
WT	Wind turbine

References

1. Lichtenegger, G.; Rentizelas, A.A.; Trivyza, N.; Siegl, S. Offshore and onshore wind turbine blade waste material forecast at a regional level in Europe until 2050. *Waste Manag.* **2020**, *106*, 120–131. [CrossRef]
2. Hevia-Koch, P.; Jacobsen, H.K. Comparing offshore and onshore wind development considering acceptance costs. *Energy Policy* **2019**, *125*, 9–19. [CrossRef]
3. International Energy Agency. *Net Zero by 2050*; OECD Publishing: Paris, France, 2021; p. 224. [CrossRef]
4. Tvinnereim, E.; Mehling, M. Carbon pricing and deep decarbonisation. *Energy Policy* **2018**, *121*, 185–189. [CrossRef]
5. European Commission . An EU Strategy to harness the potential of offshore renewable energy for a climate neutral future. In *COM(2020)*; European Commission: Brussels, Belgium , 2020.
6. WindEurope. *Our Energy, Our Future How Offshore Wind Will Help Europe Go Carbon-Neutral*; Technical Report; WindEurope: Brussels, Belgium, 2019.
7. Taylor, P.; Yue, H.; Campos-Gaona, D.; Anaya-Lara, O.; Jia, C. Wind farm array cable layout optimisation for complex offshore sites—A decomposition based heuristic approach. *Iet Renew. Power Gener.* **2023**, *17*, 243–259. [CrossRef]
8. Cerveira, A.; Baptista, J.; Pires, E.J.S. Optimization design in wind farm distribution network. In Proceedings of the International Joint Conference SOCO'13-CISIS'13-ICEUTE'13, Salamanca, Spain, 11–13 September 2013; Springer: Berlin/Heidelberg, Germany, 2014; pp. 109–119.
9. Cerveira, A.; de Sousa, A.; Pires, E.S.; Baptista, J. Optimal cable design of wind farms: The infrastructure and losses cost minimization case. *IEEE Trans. Power Syst.* **2016**, *31*, 4319–4329. [CrossRef]
10. Cerveira, A.; Pires, E.J.S.; Baptista, J. Wind farm cable connection layout optimization with several substations. *Energies* **2021**, *14*, 3615. [CrossRef]
11. Cerveira, A.; de Sousa, A.; Pires, E.J.S.; Baptista, J. Optimizing wind farm cable layout considering ditch sharing. In *International Transactions in Operational Research*; John Wiley & Sons, Inc.: Hoboken, NJ, USA, 2023. Available online: https://onlinelibrary.wiley.com/doi/pdf/10.1111/itor.13258 (accessed on 1 February 2023).
12. Fischetti, M.; Pisinger, D. Optimizing wind farm cable routing considering power losses. *Eur. J. Oper. Res.* **2018**, *270*, 917–930. [CrossRef]
13. Balakrishnan, R.K.; Hur, S.H. Maximization of the Power Production of an Offshore Wind Farm. *Appl. Sci.* **2022**, *12*, 4013. [CrossRef]

14. Shin, D.; Ko, K. Experimental study on application of nacelle-mounted LiDAR for analysing wind turbine wake effects by distance. *Energy* **2022**, *243*, 123088. [CrossRef]
15. Jensen, N.O. *A Note on Wind Generator Interaction*; Rise National Laboratory: Roskilde, Denmark, 1983.
16. Katic, I.; Højstrup, J.; Jensen, N.O. A simple model for cluster efficiency. In *European Wind Energy Association Conference and Exhibition*, A. Raguzzi: Rome, Italy, 1986; Volume 1, pp. 407–410.
17. Archer, C.L.; Vasel-Be-Hagh, A.; Yan, C.; Wu, S.; Pan, Y.; Brodie, J.F.; Maguire, A.E. Review and evaluation of wake loss models for wind energy applications. *Appl. Energy* **2018**, *226*, 1187–1207. [CrossRef]
18. Mirsane, R.S.; Torabi, F. An innovative method of investigating the wind turbine's inflow speed in a wind farm due to the multiple wake effect issue. *Energy Convers. Manag.* **2022**, *269*, 116077. [CrossRef]
19. Amaral, L.; Castro, R. Offshore wind farm layout optimization regarding wake effects and electrical losses. *Eng. Appl. Artif. Intell.* **2017**, *60*, 26–34. [CrossRef]
20. Horn , H.H. Otimização do Parque Eólico de Osório Utilizando Algorítmo Genético. Ph.D. Thesis, University of Vale do Rio dos Sinos, São Leopoldo, Brazil, 2018.
21. Zhong, C.; Wang, H.; Jiang, Z.; Tian, D. A unified optimization control of wind farms considering wake effect for grid frequency support. *Wind. Eng.* **2023**, *online first*.
22. Fischetti, M.; Pisinger, D. Mathematical optimization and algorithms for offshore wind farm design: An overview. *Bus. Inf. Syst. Eng.* **2019**, *61*, 469–485. [CrossRef]
23. Baptista, J.; Lima, F.; Cerveira, A. Optimization of Wind Turbines Placement in Offshore Wind Farms: Wake Effects Concerns. In *International Conference on Optimization, Learning Algorithms and Applications, OL2A 2021*; Revised Selected Papers; Springer: Cham, Switzerland, 2022; pp. 102–109.
24. Jesus, B.; Cerveira, A.; Baptista, J. Optimization of Offshore Wind Farms Configuration Minimizing the Wake Effect. In Proceedings of the 20th International Conference on Renewable Energies and Power Quality (ICREPQ'22), Vigo, Spain, 27–29 July 2022.
25. Anagnostopoulos, S.; Piggott, M. Offshore wind farm wake modelling using deep feed forward neural networks for active yaw control and layout optimisation. In *Journal of Physics: Conference Series*; IOP Publishing: Bristol, UK, 2022; Volume 2151, p. 012011.
26. Aukitino, T.; Khan, M.G.; Ahmed, M.R. Wind energy resource assessment for Kiribati with a comparison of different methods of determining Weibull parameters. *Energy Convers. Manag.* **2017**, *151*, 641–660. [CrossRef]
27. Celik, A.N. A statistical analysis of wind power density based on the Weibull and Rayleigh models at the southern region of Turkey. *Renew. Energy* **2004**, *29*, 593–604. [CrossRef]
28. Bowden, G.; Barker, P.; Shestopal, V.; Twidell, J. The Weibull Distribution Function and Wind Power Statistics. *Wind. Eng.* **1983**, *7*, 85–98.
29. Ali, S.; Lee, S.M.; Jang, C.M. Statistical analysis of wind characteristics using Weibull and Rayleigh distributions in Deokjeok-do Island—Incheon, South Korea. *Renew. Energy* **2018**, *123*, 652–663. [CrossRef]
30. Justus, C.; Mikhail, A. Height variation of wind speed and wind distributions statistics. *Geophys. Res. Lett.* **1976**, *3*, 261–264. [CrossRef]
31. Wade, B.M. Investigation of Offshore Wind Farm Layout Optimization Regarding Wake Effects and Cable Topology. Ph.D. Thesis, Instituto Superior Técnico, Lisboa, Portugal, 2018.
32. Amar, F.B.; Elamouri, M. Wind energy assessment of the sidi daoud wind farm-Tunisia. In *Wind Farm-Technical Regulations, Potential Estimation and Siting Assessment*; IntechOpen: Rijeka, Croatia, 2011; pp. 115–140.
33. Saraiva, R. Localização Óptima dos Conversores de um Parque Eólico Para Minimização de Custos Totais. Master's Thesis, Instituto Superior Técnico, Lisbon, Portugal, 2007.
34. Al Shereiqi, A.; Mohandes, B.; Al-Hinai, A.; Bakhtvar, M.; Al-Abri, R.; El Moursi, M.; Albadi, M. Co-optimisation of wind farm micro-siting and cabling layouts. *IET Renew. Power Gener.* **2021**, *15*, 1848–1860. [CrossRef]
35. Frandsen, S. On the wind speed reduction in the center of large clusters of wind turbines. *J. Wind. Eng. Ind. Aerodyn.* **1992**, *39*, 251–265. [CrossRef]
36. Rodrigues, S. A Multi-Objective Optimization Framework for the Design of Offshore Wind Farms. Ph.D. Thesis, Delft University of Technology, Delft, The Netherlands, 2016.
37. Hansen, T.H. Offshore Wind Farm Layouts. Ph.D. Thesis, Norwegian University of Science and Technology, Trondheim, Norway, 2009.
38. Green, J.; Bowen, A.; Fingersh, L.J.; Wan, Y.H. Electrical collection and transmission systems for offshore wind power. In *Offshore Technology Conference*; OnePetro: Richardson, TX, USA, 2007.
39. Nexans. Integrated Cable Solutions for Offshore Wind Development. Available online: https://www.nexans.pt (accessed on 1 February 2023). .
40. Qi, Y.; Hou, P.; Yang, L.; Yang, G. Simultaneous optimisation of cable connection schemes and capacity for offshore wind farms via a modified bat algorithm. *Appl. Sci.* **2019**, *9*, 265. [CrossRef]
41. Shen, X.; Wu, Q.; Zhang, H.; Wang, L. Optimal Planning for Electrical Collector System of Offshore Wind Farm with Double-sided Ring Topology. *IEEE Trans. Sustain. Energy* **2023**, *14*, 1624–1633. [CrossRef]
42. Paul, S.; Rather, Z.H. A novel approach for optimal cabling and determination of suitable topology of MTDC connected offshore wind farm cluster. *Electr. Power Syst. Res.* **2022**, *208*, 107877. [CrossRef]

43. FICO Xpress. Xpress Optimization. Available online: https://www.fico.com/en/products/fico-xpress-optimization (accessed on 1 February 2023).
44. Wind Turbine Models. Available online: https://en.wind-turbine-models.com/turbines/318-vestas-v164-8.0 (accessed on 1 February 2023).
45. BVGAssociates. Wind Farm Cost. Available online: https://guidetoanoffshorewindfarm.com/wind-farm-costs (accessed on 1 February 2023).
46. Global Wind Atlas. Available online: https://globalwindatlas.info/en (accessed on 1 February 2023).
47. Smail, H.; Alkama, R.; Medjdoub, A. Optimal design of the electric connection of a wind farm. *Energy* **2018**, *165*, 972–983. [CrossRef]
48. Insights, S.G.C. Benchmark UK Offshore Wind Load Factors Seen Rising to 57% in 2030: BEIS. March 2023. Available online: https://www.spglobal.com (accessed on 1 February 2023).
49. Trinomics, B. *Final Report Cost of Energy (LCOE): Energy Costs, Taxes and the Impact of Government Interventions on Investments*; European Union: Brussels, Belgium, 2020.